Development of Gold Contacted Flip-chip Detectors with IMARAD CZT

T. Narita[1], P.F. Bloser[1], J.E. Grindlay[1], J.A. Jenkins [1]

[1]Harvard-Smithsonian Center for Astrophysics, 60 Garden St., Cambridge, MA 02138

ABSTRACT

We present initial results from our evaluation of a gold-contacted pixellated detector using cadmium zinc telluride substrate produced by IMARAD Imaging Systems. The Horizontal Bridgman (HB) grown crystals from IMARAD have been shown to produce high resolution photopeaks, but they are also seen to have large leakage current. Our previous tests with IMARAD CZT showed that the use of indium anodes and gold cathode improved the resistivity compared to the standard indium-contacted detectors. We seek to test whether simple evaporated gold contacts alone could also reduce the leakage current and thus improve the spectral resolution, especially in the 10-100 keV energy range. We have fabricated several metal-semiconductor-metal (MSM) detectors with a 4×4 array of pixels on 10×10 mm substrates. Measurements of the detectors' leakage current, spectral response, and temperature sensitivity are presented and compared to IMARAD's ohmic contact detector and gold contact MSM detectors made of High Pressure Bridgman (HPB) material. Finally, we show preliminary results from a tiled flip-chip pixellated detector made using the IMARAD detectors.

Keywords: CdZnTe, pixellated imaging detectors, hard X-ray imaging

1. INTRODUCTION

Due to the considerable potential shown by Cadmium Zinc Telluride (CZT) in the past several years, the next generation of astronomical high energy X-ray satellites (Swift, Constellation-X, EXIST) will almost certainly employ CZT as their hard X-ray detectors. The advantages of CZT are numerous: operation at room temperature due to its large bandgap, effective stopping power at reasonable thickness, and the lack of polarization effects typically found in CdTe. A variety of electrode designs have also been developed to compensate for the poor hole mobility, and one can now obtain much better energy resolution from CZT than from scintillators. These favorable material characteristics and the new readout designs have made CZT a promising semiconductor for medical and nuclear technologies, in addition to astronomy. For a mission such as EXIST,[1] where the detector area approaches ten square meters, major issue is the increase in yield of large volume spectroscopic grade material. Currently the High Pressure Bridgman (HPB) growth process produces high resistivity (10^{11} ohm-cm) material which is relatively free of structural defects. However, the yield of HPB crystals with dimensions greater than 10×10 mm^2 and free of macroscopic defects is low. Fabrication of large area detectors will require tiling many smaller modules and thus the availability of large volume crystals is essential.

IMARAD Imaging Systems produces CZT which is grown using a modified Horizontal Bridgman (HB) process.[2] This method produces large area crystals (40×40 mm^2) which are relatively free of defects. Pixellated detectors made with IMARAD material have been characterized and found to have uniform leakage current and spectroscopic response across pixels.[3,4] By using larger crystals, the problems associated with tiling detector modules into a large area array are greatly simplified. However, one drawback of the HB process is that the crystals are typically lower in resistivity than those made with the HPB process. A pixellated IMARAD detector which uses indium for the electrodes has a typical resistivity of about 5×10^9 ohm-cm.[5] While low resistivity is not critical for spectroscopy at X-ray energies greater than 100 keV, the large leakage current significantly degrades the energy resolution at 5-60 keV.

One method to decrease the leakage current of a detector, and thus improve the spectral resolution, is the addition of blocking contacts. Recent tests using gold cathode and either CdS or In anodes on IMARAD material showed an increase in the reverse bias resistivity.[4] We speculated that the gold electrode acted as a blocking contact when

Further author information: (Send correspondence to T. Narita)
tnarita@cfa.harvard.edu

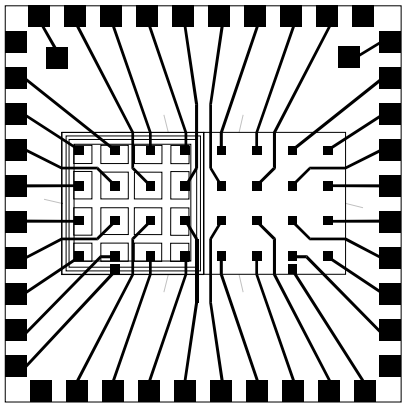

Figure 1. The pixel side layout is sketched for one of the tiled flip-chip detectors. The traces and pads are explained in Section 2.6

used with IMARAD material, and thus it would be a simple process to improve the detector performance. In this paper, we report our preliminary results from gold pixellated detectors made with IMARAD and eV Products CZT. We compared the resistivity, spectral response, and the low temperature performance of these detectors. We also present results from our tiled flip-chip detector.

2. DETECTOR DEVELOPMENT

2.1. Detectors

We fabricated two gold contacted detectors using $10 \times 10 \times 5$ mm^3 CZT samples from IMARAD (hereafter called IMARAD-Au) and two gold contacted detectors of the same dimension with HPB CZT from eV Products (hereafter called eV Products-Au). The detectors were processed at RMD in Watertown, MA. To insure uniformity, one IMARAD crystal and one eV Products crystal were each placed side by side in the evaporation chamber during fabrication. Evaporated gold was used for the electrodes, and a shadow mask was used for the pixel definition.

Each detector was made with a 4×4 array of pixels surrounded by a 0.55 mm guard ring. In order to preserve the pixel pitch of 2.5 mm, the center four pixels were 2.35 mm square and the four corner pixels were 1.725 mm square. The eight side pixels have a rectangular shape of 2.35 by 1.725 mm. The gaps between pixels, and between pixels and guard ring, were 150μm. A sketch of the detector pixel layout is shown in Figure 1. We also tested a standard detector from IMARAD. It was a $20 \times 20 \times 4$ mm crystal with an array of 8×8 1.9 mm indium-contacted pixels. The pixel pitch was identical to the 4×4 array gold-contacted detectors at 2.5 mm. The cathode plane also used indium.

2.2. Leakage Current

We first characterized the detectors by measuring the single-pixel leakage current as a function of bias voltage. The reverse bias resistivity was then calculated at a typical operating voltage of -700 volts. We list the averaged single pixel resistivities in Table 1. A 3×3 array of spring-loaded pogo pins with conductive rubber tips was used to contact each detector. By grounding the exterior eight pins, we were able to isolate the leakage current to that of one center pixel. We used a Canberra high voltage supply and a Keithley 237 as an ammeter. All measurements were taken in the dark and at room temperature. Figure 2 shows the I-V curves taken from a sample pixel of the same geometric size on the IMARAD-Au and eV Products-Au detectors, and the I-V curve from the standard IMARAD detector. Since the pixel sizes and crystal thickness vary between the IMARAD standard detector and the new gold contacted detectors, the I-V curves alone do not indicate the difference in resistivities. However, one can clearly see the qualitative difference in the current-voltage relation between the detectors.

Detector	Resistivity	σ
IMARAD-Au	9.9	0.28
eV Products-Au	10.9	0.45
standard IMARAD	1.0	0.2

Table 1. Averaged reverse bias resistivity at -700 V, in units of 10^{11} ohm-cm. The σ indicates the empirically measured rms scatter in the data.

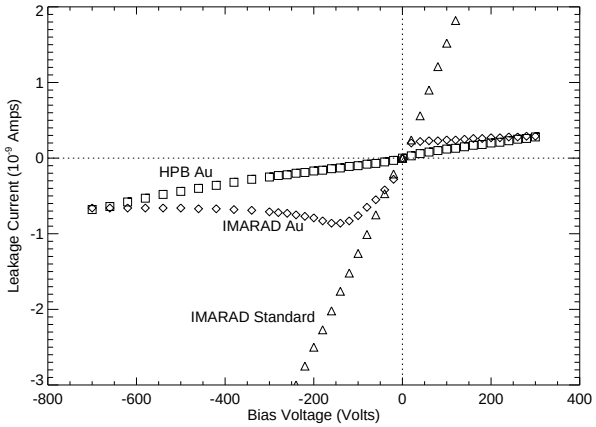

Figure 2. Sample single pixel I-V curves for IMARAD-Au, eV Products-Au, and standard IMARAD are plotted. The gold contacted IMARAD detector shows diode-like curves while the eV Products-Au detector and standard IMARAD detector show linear curves.

The IMARAD standard detector and the eV Products-Au detectors both exhibited linear I-V curves, while the IMARAD-Au detectors showed a diode-like I-V curve. This indicates that the IMARAD material is probably n-type since it forms an ohmic contact with a low work function metal such as indium, while it forms a blocking contact with high work function metal such as gold. By using blocking contacts, the reverse bias resistivity of the IMARAD-Au detector increased by a factor of ten compared to the standard IMARAD detector. The IMARAD-Au resistivity was comparable to that of the eV Products-Au detector at -700 V. Furthermore, the flatter slope of the I-V curve shows that lower leakage current may be possible with the gold contacted IMARAD detector than with eV Products detector at bias greater than -700 V.

2.3. Energy Resolution

The spectral resolution of the detectors, consisting of photopeak FWHM and photopeak efficiency, was measured using a non-collimated ^{57}Co source. The test fixture consisted of an array of spring-loaded pins contacting the detector. The outside neighbor pixels were shorted to ground while the center pixel was read out by a low noise eV Products 550 preamp. The preamp output was shaped at 1 μs time constant and recorded by an MCA. Typical center pixel ^{57}Co spectra are shown in Figure 3 for the IMARAD-Au and eV Products-Au detectors. The detectors were all biased at -700 V. Each spectrum was fit with a Gaussian photopeak and an exponential low energy tail. At -700 V bias, the average center pixel photopeak FWHM energy resolutions (with no corrections) were $4.2 \pm 0.6\%$ and $5.5 \pm 0.6\%$, respectively for IMARAD-Au and eV Products-Au. The empirically observed rms scatter in the FWHM were reported as errors (4 center pixels from 4 detectors). The photopeak efficiency was defined as the ratio of the counts in the Gaussian to the total counts in the range of $+2.35\sigma$ above and -5σ below the photopeak center. The averaged efficiencies were $64.2 \pm 2.5\%$ and $76.1 \pm 2.9\%$ for IMARAD-Au and eV Products-Au detectors, respectively.

We found that the energy resolution was slightly better with the IMARAD-Au detector than with the eV Products-Au detector. This was surprising given that the pixel leakage currents were similar at the operating bias of -700 V, and identical readout electronics were used on both types of detectors. The difference in the photopeak FWHM was

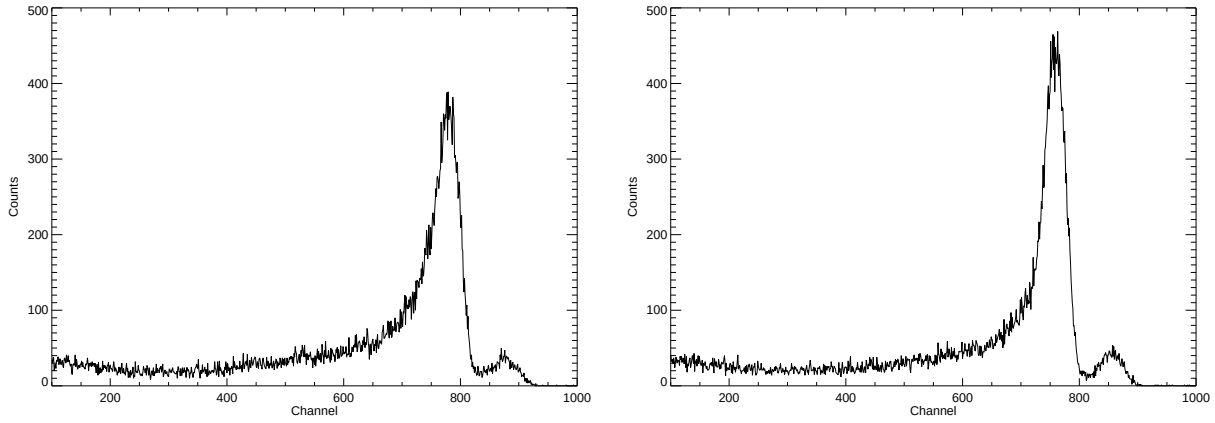

Figure 3. ^{57}Co spectra taken with eV Products-Au (left) and IMARAD-Au (right) detectors at -700 V bias.

Detector	FWHM Energy Resolution (^{57}Co)	σ	Photopeak Efficiency	σ
IMARAD-Au	4.2%	0.6%	76.1%	2.9%
HPB Au	5.5%	0.6%	64.2%	2.5%

Table 2. Average energy resolution and photopeak efficiency from ^{57}Co spectra taken with IMARAD-Au and eV Products-Au detectors. The FWHM values are comparable between detectors, but the IMARAD-Au detectors have significant improvement in the photopeak efficiency.

due to the smaller low energy tail in the IMARAD-Au detector, which had a significantly better photopeak efficiency than the eV Products-Au detector.

We investigated this further by measuring the signal induced on the anode electrode as a function of the X-ray interaction depth. This was done by digitizing both the anode and the cathode signal for each X-ray event.[6] While this was not the first use of this technique to study pixellated devices,[7] our study is the first to compare the performance across two detectors of identical pixel geometry. For the anode pixel readout, we used the same spring loaded pins to contact the center pixel while grounding the neighbor pixels. The anode signal was then amplified with an eV Products 550 preamp and shaped with 1μs time constant. The cathode signal was also read out by a second eV Products 550 preamp and shaped with 1μs time constant. The shaped anode pulse was used as the trigger to hold both the anode and cathode pulse heights, which were then digitized with a 12 bit ADC and recorded by a computer. In Figure 4, the top two panels display a typical anode versus cathode scatter plot showing the induced signal on the anode as a function of the interaction depth. The vertical axis shows the cathode pulse height and the horizontal axis shows the anode pulse height. The set of points on a curved track shows the pulse heights from 122 keV X-ray photons. The curvature of the photopeak track is a function of the weighting potential and the amount of charge trapping. Since the IMARAD-Au and eV Products-Au detectors have the same pixel geometry, and thus the same weighting potential, any difference in the curvature between the detector types must be due to the CZT material properties.

In Figure 4, the bottom two panels show the projection of the anode versus cathode scatter plot as a spectrum for each detector. The induced anode signal from the IMARAD-Au detectors was found to be less dependent on the interaction depth. This is seen in the photopeak track which is more vertical for the IMARAD-Au detectors than for the eV Products detectors. This results in a spectrum with less tailing and better photopeak efficiency. The insensitivity of the anode to the interaction depth is a key feature of using pixellated devices (small pixel effect[8]). However, it can also be tuned by decreasing the number of electrons moving through the nearly full thickness of the detector. By trapping some of the electrons generated nearest the cathode, which would have otherwise induced the largest amount of charge on the anode, the amount of induced anode signal could be made more or less equal for a range of X-ray interaction depths near the cathode. An adjustment in the detector bias voltage can increase the

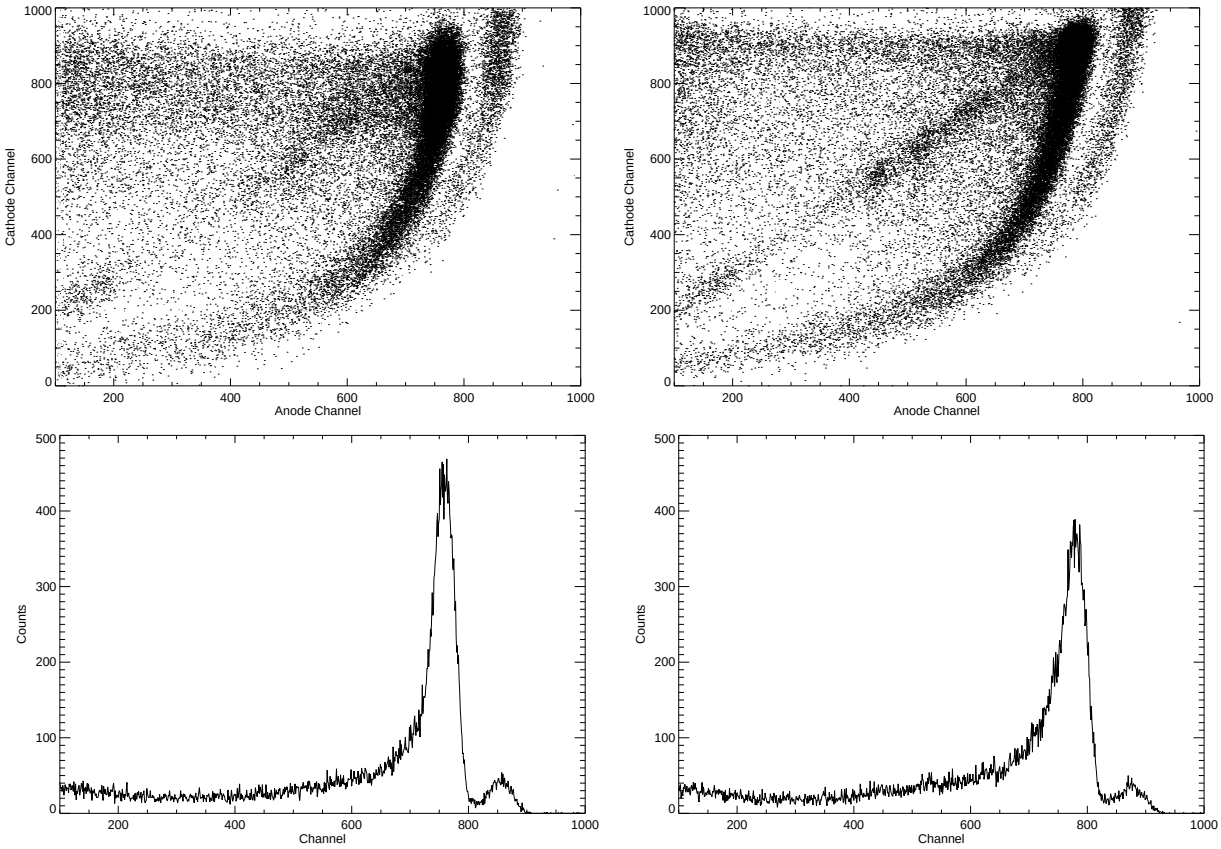

Figure 4. Comparison of the anode versus cathode scatter plot between IMARAD-Au and eV Products-Au detectors. The left column shows the scatter plot and the resulting spectrum for IMARAD-Au, and the right column shows the same for eV Products-Au. The photopeak track seen in the scatter plot is typically more vertical for IMARAD-Au, and its projection on the anode axis results in a less tailed spectrum.

electron drift time, leading to more trapping. In our case, the two types of detectors shared the same pixel geometry and were measured using the same bias voltage. Thus we speculate that the enhanced photopeak efficiency of the IMARAD-Au detector must be due to the lower electron mobility in the IMARAD material.

2.4. Detector Efficiency

In the past several years, we have experimented with PIN contacts on CZT to improve the reverse bias resistivity of the material.[9] However, PIN detectors typically suffer from non-depleted regions where the low electric field limits the movement of the charge carriers and the X-ray events are lost or degraded. With our gold-contacted detectors, we compared the active volume of the IMARAD-Au and eV Products-Au detectors by measuring the detection efficiency of 122 keV photons. For this test, we used a calibrated ^{57}Co beam and recorded the count rate in the center pixels of the detectors. The efficiency was defined as the total number of counts in the spectrum falling between -5σ and $+2.35\sigma$ of the photopeak center. We recorded the efficiency of each center pixel and averaged them for both detector types. By dividing the averaged IMARAD-Au efficiency by the eV Products-Au efficiency, we derived a relative efficiency between the two detector types of 1.35 ± 0.28. Although better statistics are needed, our measured relative detector efficiency is consistent with one. We thus conclude that there is no difference in the detectors' active volumes, at least up to 122 keV.

2.5. Temperature Sensitivity

CZT detectors in space missions may be subject to some variation in temperature unless active thermal control systems are employed. Thus, we are interested in the performance of these detectors in the temperature range of

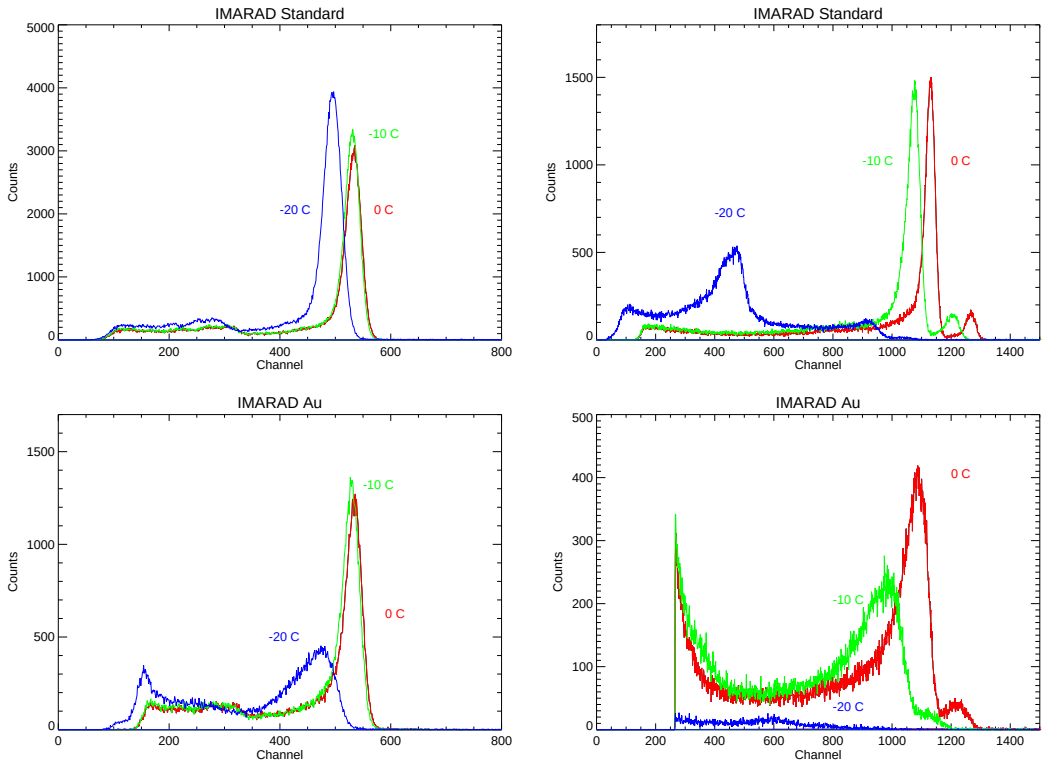

Figure 5. ^{241}Am (left column) and ^{57}Co (right column) spectra taken with IMARAD standard and IMARAD-Au detectors at 0, -10, and -20°.

$-20°$ to $+20°$ C. To study the temperature sensitivity of IMARAD detectors, we placed the IMARAD-Au detector and the IMARAD standard detectors in a thermal chamber, cooled them to $-20°$ Celsius, and recorded ^{241}Am and ^{57}Co spectra. The test fixture used the same spring-loaded pin array and the low noise preamp for measuring energy resolution at room temperature. The shaping time was fixed at 1μs. The entire electronic readout system was cooled along with the detectors, and the temperature of the detector was measured by a thermistor attached to the test fixture. To minimize the thermal shock to the CZT, the cooling chamber was controlled such that the temperature slew of the detector fixture was about one degree per minute.

Each spectrum was integrated for one minute while the temperature of the detector stayed constant within $\pm 1°$ C. The detectors were all biased at -700 V. Figure 5 shows a mosaic of spectra taken with IMARAD standard and IMARAD-Au detectors, at 0, -10, and $-20°$Celsius. For the standard IMARAD detector, the photopeak gain decreased with lower temperature, but interestingly the ^{241}Am photopeak count rate increased from $-10°$ to $-20°$. This was not the case for the ^{57}Co spectrum where the 122 keV photopeak degraded below $-10°$. The photopeak degradation was even more apparent for the IMARAD-Au detector. The ^{241}Am photopeak was severely degraded below $-10°$, and the 122 keV photopeak had almost disappeared at $-20°$ in a manner similar to the polarization effects found in CdTe detectors. Although we are currently investigating the low temperature behavior in more detail, we speculate that these effects are caused by an increase in the electron detrapping time. Such an effect would result in a poor spectrum due to incomplete charge collection and ballistic deficit for the 1μs shaping time used.

2.6. Flip-chip Detector

As a preliminary step to building a tiled large area detector, we fabricated and tested two tiled flip-chip detector modules using one IMARAD-Au detector and one eV Products-Au detector on each module. Each detector module required a thin Alumina substrate board with an array of 4×8 gold pixel pads at 2.5 mm pitch. Wire bond gold studs were placed in the center of each pad. Additional pads were placed for the guard ring and the high voltage

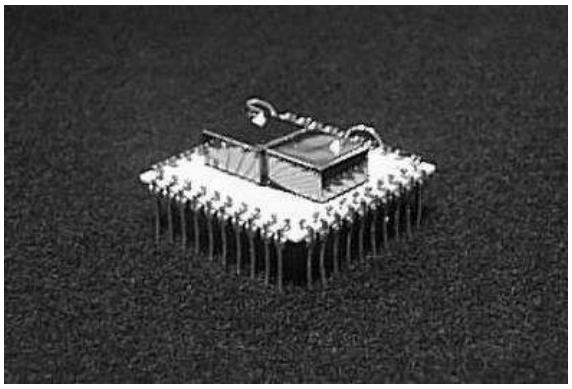

Figure 6. Tiled flipchip detector array on a readout board. The wires connect the high voltage pads to the cathode plane.

connections. Fanout traces connected the internal pads to the edge pads, where clip-pins were soldered. A sketch of the Alumina board is shown in Figure 1. The two crystals were visually aligned and bonded in a tiled manner onto the pixel pads using conductive epoxy. After a low temperature curing cycle, a non-conductive epoxy underfill was used for additional adhesion. A picture of the detector module is shown in Figure 6. The entire process was done at HyComp, Inc. in Marlborough, MA.

Due to unforeseen problems in the fabrication process, three pixels on the first flip-chip module IMARAD-Au detector developed shorts. Even more IMARAD-Au pixels were shorted on the second flip-chip module, rendering it unusable. Although the cause is not clear, we speculate that it was due to surface oxidation, preferentially on IMARAD CZT, from the underfill epoxy which produced partially conductive paths. The behavior of the remaining channels was normal. The detector module is readout by a 32-channel VA/TA ASIC made by IDE AS. One detector module and the support electronics will be flown on a balloon payload in September 2000 to measure the hard X-ray background spectrum at 125,000 feet. More detailed performance and simulation results from the first flip-chip module are given in Bloser et al. 2000[10]

3. CONCLUSIONS

In order to realize the goal of developing a large area hard X-ray detector for astronomy, the yield of spectroscopic grade large area detectors must be increased. Current crystal growth processes using the HPB technique result in CZT with high resistivity but relatively low yield, whereas the HB growth process has high yield but low resistivity. To compensate for the low resistivity in HB CZT, we have fabricated and tested pixellated detectors using gold blocking contacts on IMARAD CZT.

By using simple evaporated gold electrodes, the operating bias resistivity was increased by an order of magnitude compared to the IMARAD detectors made without the blocking contacts. The resistivity of the gold-contacted IMARAD detector was comparable with that of the higher resistivity HPB CZT detectors when both detectors were biased at -700 V. The spectra taken with the IMARAD-Au detector showed excellent photopeak efficiency, and this was probably due to higher level of electron trapping in the IMARAD CZT compared to the HPB CZT from eV Products. A similar effect might also result from a detector with a low bias region near the cathode, but we found no difference in the detector efficiency between IMARAD-Au and eV Products-Au detectors using a calibrated ^{57}Co source. We did find however, that the IMARAD detectors performed poorly when they were cooled to below -10° Celsius. We speculate that this is a further increase in the high level of electron trapping in the material. Finally, we fabricated and tested a tiled flip-chip detector for use in our hard X-ray balloon-borne experiment. The detector, comprising one IMARAD-Au and one eV Products-Au detector, will be flown in September 2000, and the results will be given in a future paper.

ACKNOWLEDGMENTS

We thank Dr. Uri El-Hanany of IMARAD Imaging Systems and Kevin Parnham at eV Products for supplying us with CZT samples. We thank Kanai Shah and Paul Bennett at RMD Inc. for their assistance in detector fabrication. Finally, we thank George Riley at HyComp, Inc. for his assistance in the flipchip processing. This work was supported in part by NASA grants NAG5-5103 and NAG5-5209.

REFERENCES

1. J. Grindlay et al., "EXIST: a high sensitivity hard x-ray imaging sky survey mission for ISS," in *Fifth Compton Symposium*, M. McConnell and J. Ryan, eds., *AIP Conf. Proc.* **510**, p. 784, 1999.
2. P. Cheuvart, U. El-Hanany, D. Schneider, and R. Triboulet *J. Crystal Growth* **101**, 1990.
3. T. Schlesinger, B. Brunett, H. Yao, J. VanScyoc, R. James, S. Egarievwe, K. Chattopadhyay, X. Ma, A. Burger, N. Giles, U. El-Hanany, A. Shahar, and A. Tsigelman, "Large volume imaging arrays for gamma-ray spectroscopy," *Presented at II-VI Workshop* , 1998.
4. T. Narita, P. Bloser, J. Grindlay, J. Jenkins, and H. Yao, "Development of IMARAD CZT detectors with PIN contacts," in *Hard X-Ray, Gamma-Ray, and neutron detector physics*, R. James and R. Schirato, eds., *Proc. SPIE* **3768**, p. 55, 1999.
5. U. El-Hanany *Private Communication* .
6. A. Shor, Y. Eisen, and I. Mardor, "Spectroscopy with CdZnTe γ and x-ray detectors," *NIM* **403**, p. 417, 1999.
7. T. Schlesinger, M. Greaves, S. Ross, B. Brunett, J. V. S. III, and R. James, "Role of uniformity and geometry in IMARAD-type gamma-ray spectrometers," in *Hard X-Ray, Gamma-Ray, and neutron detector physics*, R. James and R. Schirato, eds., *Proc. SPIE* **3768**, p. 16, 1999.
8. H. Barrett and J. Eskin, "Charge transport in arrays of semiconductor gamma-ray detectors," *Phys. Rev. Lett.* **75**, pp. 156–159, 1995.
9. T. Narita, P. Bloser, J. Grindlay, R. Sudharsanan, C. Reiche, and C. Stenstrom, "Development of prototype pixellated PIN CdZnTe detectors," in *Hard X-Ray and Gamma-Ray Detector Physics and Applications*, F. Doty and R. Hoover, eds., *Proc. SPIE* **3446**, p. 218, 1998.
10. P. Bloser, J. Grindlay, J. Jenkins, and T. Narita, "Construction and testing of a pixellated CZT detector and shield for a hard x-ray astronomy balloon flight," in *X-ray and Gamma-ray instrumentation for Astronomy*, K. Flanagan and O.H.W.Siegmund, eds., *Proc. SPIE* **4140**, 2000.